

# A Combined Experimental and Computational Study on the Shuttle Mechanism of Piperazine for the Enhanced CO<sub>2</sub> Absorption in Aqueous Piperazine Blends

Qinlan Luo, Qulan Zhou, Bin Feng, Na Li,\* and Shicheng Liu



Cite This: *Ind. Eng. Chem. Res.* 2022, 61, 1301–1312



Read Online

ACCESS |



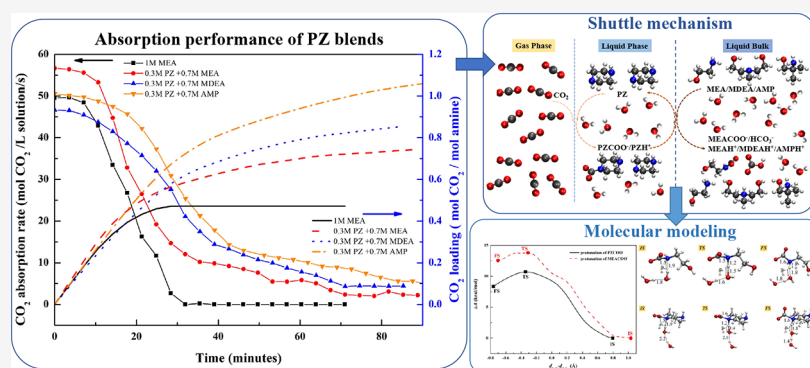
Metrics & More



Article Recommendations



Supporting Information



**ABSTRACT:** Piperazine (PZ) blends containing PZ and monoethanolamine (MEA)/N-methyldiethanolamine (MDEA)/2-amino-2-methyl-propanol (AMP) were experimentally and computationally investigated to analyze their potential capabilities for CO<sub>2</sub> capture, and the shuttle mechanism of PZ for enhanced CO<sub>2</sub> absorption were verified. In experiments, the concentration of both PZ and MEA/MDEA/AMP were varied to show the effect of concentration ratio and the influence of amine components on the CO<sub>2</sub> absorption rate and capacity. Experimental results showed that all the PZ blends possessed high absorption rates and large absorption capacities. To further understand the interaction behavior of amines/products and possible reaction pathways, both qualitative and quantitative <sup>13</sup>C NMR analyses were conducted. The results indicated the conversion between absorption products, which can release free PZ to capture CO<sub>2</sub> and consequently improve the absorption performance. Moreover, the static quantum mechanical calculations and ab initio molecular dynamics (AIMD) simulations combined with metadynamics sampling were conducted to evaluate the thermodynamic stability of absorption products and kinetically favorable key elementary reactions in PZ blends. This study highlights an accurate description of the shuttle effect of PZ for the enhanced CO<sub>2</sub> capture by PZ blends.

## INTRODUCTION

Carbon dioxide (CO<sub>2</sub>) capture has gained worldwide attention as the greenhouse effects have become more and more serious in recent years. The chemical absorption using aqueous amine solutions is one of the most effective and economical technologies for CO<sub>2</sub> capture<sup>1</sup> compared to other alternative technologies, such as oxy-combustion, membrane separation, and physical adsorption.<sup>2</sup> The most commonly used amines include primary amine (monoethanolamine, MEA), secondary amine (diethanolamine, DEA), tertiary amine (N-methyldiethanolamine, MDEA), diamine (piperazine, PZ), and steric hindered amine (2-amino-2-methyl-propanol, AMP). Investigations on the relationship between the molecular structure and amine activity have provided a fundamental guide for CO<sub>2</sub> absorption using single amine solutions.<sup>3</sup> It is known that primary amine and secondary amine have high reaction activity and fast absorption rate, while the tertiary amine and sterically hindered amine have large absorption capacity and low

regeneration energy consumption.<sup>4</sup> Therefore, the blends of primary and tertiary/steric hindered amines or secondary and tertiary/steric hindered amines have attracted attention in recent years, which offer enhanced absorption rate/capacity and reduced energy consumption for regeneration.<sup>5</sup>

Some experimental studies indicated that PZ showed a perfect performance in CO<sub>2</sub> absorption,<sup>6</sup> with the double CO<sub>2</sub> absorption rate and capacity compared to the equal concentration of MEA.<sup>7</sup> However, it has the disadvantages of low solubility in aqueous solutions, the problem of easy crystallization, and also high energy consumption for

**Received:** October 19, 2021

**Revised:** December 30, 2021

**Accepted:** December 30, 2021

**Published:** January 12, 2022



regeneration. The addition of PZ in aqueous alkanolamines (e.g., AMP or MDEA) has been suggested for more efficient CO<sub>2</sub> removal,<sup>8</sup> which can accelerate CO<sub>2</sub> absorption, improve CO<sub>2</sub> loading, reduce amine volatility, and relieve the solid precipitation of concentrated PZ or PZ-carbamate (PZCOO<sup>-</sup>). Therefore, ongoing research is investing in new PZ blends requiring high absorption rate, high CO<sub>2</sub> capacity, and no precipitation during CO<sub>2</sub> absorption.<sup>9</sup>

Earlier studies on PZ blends focused on the improvement of CO<sub>2</sub> absorption performance. Nwaoha et al.<sup>10,11</sup> have compared the absorption capacity, the heat of absorption, and the regeneration energy consumption of aqueous PZ + AMP and MEA + AMP + PZ systems, and their results indicated that the aqueous MEA + AMP + PZ showed a higher absorption capacity and the avoidance of precipitate formation. Du et al.<sup>12</sup> have studied the CO<sub>2</sub> absorption rate and capacity of 21 novel tertiary and hindered amines blended with PZ and also investigated the effect of structural features of tertiary and hindered amines on the absorption performance. However, the fundamental mechanisms under the improved absorption performance of PZ blends are rarely reported, which can play a directive role in the development of new PZ blends. Some people raised the “shuttle mechanism”,<sup>13</sup> whereby the PZCOO<sup>-</sup> tends to be formed at the gas–liquid surface and further regenerates CO<sub>2</sub> in the bulk solution, which can then react with other amines, leasing free PZ to diffuse to the surface to capture CO<sub>2</sub> again. Nevertheless, Puxty and Rowland<sup>14</sup> pointed out that enhanced mass transfer in PZ mixtures can be explained through chemical interactions occurring in the mixtures without the need to resort to the “shuttle mechanism”.

To understand the reaction mechanisms underlying in CO<sub>2</sub> absorption into aqueous PZ blends, the reliable estimation of the liquid phase composition or speciation of CO<sub>2</sub>-amines-H<sub>2</sub>O systems is the first essential step. Nuclear magnetic resonance (NMR) techniques have been widely used for the qualitative identification and quantitative determination of the concentration of species to identify the probable reactions and the possible interconversion between species. Zhang et al.<sup>4</sup> used the <sup>13</sup>C NMR spectroscopy to quantify species formed in the MEA-MDEA-PZ solutions with varying CO<sub>2</sub> loading. In Lee et al.'s study,<sup>15</sup> the <sup>13</sup>C and <sup>15</sup>N NMR spectroscopy had been conducted for the identification of carbamate species and the unveiling of the dynamic equilibrium among product species of the CO<sub>2</sub> absorption by hydrazine. Ciftja et al.<sup>16</sup> had used the NMR techniques to study the formation of carbamate and to evaluate the apparent carbamate stability in the AMP-CO<sub>2</sub>-H<sub>2</sub>O system. Their results pointed out that it was possible to apply the NMR method onto the complex PZ-amines-CO<sub>2</sub>-H<sub>2</sub>O systems for the identification and confirmation of absorption products.

Besides the experimental analysis techniques, the computational study can provide molecular insights into fundamental mechanisms of the enhanced rate of CO<sub>2</sub> absorption in PZ blends. Static quantum mechanical (QM) calculations with various implicit solvation models have been employed to assess the thermodynamics stability of absorption products and the interactions between reactants in CO<sub>2</sub> absorption.<sup>17–19</sup> Zhang et al.<sup>20</sup> had used a similar approach to explore the interactive effect between different amines in the MEA/PZ/AMP/DEA binary solutions. Meanwhile, these methods have so far been unable to predict reasonable standard free energy differences and barriers of CO<sub>2</sub> absorption in aqueous solutions.<sup>21</sup> This is

because in the implicit solvation models, the aqueous environment has been treated with various dielectric continuum approximations, through which some important aspects of the aqueous environment cannot be taken into account, like the direct solute–solvent interactions,<sup>22</sup> solution structural and dynamics effects,<sup>23</sup> the steric hindrance effect of amines, and so on. Kubota and Bucko,<sup>22</sup> Andreoni's group,<sup>24,25</sup> and Hwang's group<sup>26,27</sup> have proposed the metadynamics approaches combined with ab initio molecular dynamics (AIMD) simulations to predict the overall free-energy differences and free-energy barriers for elementary reactions of CO<sub>2</sub> absorption in amine solutions, which were reasonable compared to the experimentally estimated values. However, we still lack the fundamental understanding of the enhanced absorption rate of PZ blends for CO<sub>2</sub> capture, which may aid in the development of PZ blends with better absorption and desorption performance.

In this study, experiments of CO<sub>2</sub> absorption in PZ + MEA, PZ + MDEA, and PZ + AMP solutions with different concentration ratios of PZ and MEA/MDEA/AMP were conducted to comprehensively investigate the roles of PZ in the PZ-amine-CO<sub>2</sub>-H<sub>2</sub>O systems. In addition, the absorption products in PZ + MEA, PZ + MDEA, and PZ + AMP solutions were analyzed by using quantitative <sup>13</sup>C NMR, as well as the concentration of those products with the increasing of the CO<sub>2</sub> loading. Finally, the fundamental mechanisms underlying the CO<sub>2</sub> absorption in PZ blends based on both experimental study and ab initio molecular dynamics (AIMD) simulation were also proposed to interpret the CO<sub>2</sub> absorption and desorption process in PZ blends, including both kinetic effect and thermodynamic effect.

## ■ EXPERIMENTAL SETUP

**Absorption Experiments.** Analytical grade MEA (99%, Aladdin), MDEA (99%, Aladdin), AMP (99%, Aladdin), and PZ (99%, Aladdin) were directly used without further purification. The carbon dioxide and nitrogen gas (purity 99.99%) were purchased from Xi'an Tianze Gas Co., Ltd.

The lab-scale bubbling reactor was used for the CO<sub>2</sub> absorption, and the experimental system was similar to that in our previous work.<sup>28,29</sup> The simulated flue gas with the CO<sub>2</sub> volume concentration of 18% and with the flow rate of 1 L/min was used. The CO<sub>2</sub> concentration in the inlet gas and the outlet gas were measured and recorded with a Fourier transform infrared gas analyzer (Gasmet, Dx4000, Finland). Details of the experimental system and the experimental process can be found in our previous work. Each experiment was conducted at least thrice.

The aqueous amine solutions were prepared in equivalent mole concentrations and with different concentration ratios of PZ and MEA/MDEA/AMP. The absorption rate and the CO<sub>2</sub> loading were determined at different amine components and different amine ratios of PZ blends.

**NMR Tests.** Both qualitative and quantitative <sup>13</sup>C NMR tests for PZ blends, using a Bruker Avance III 400 NMR spectrometer with the frequency of 100.62 MHz, were conducted to analyze their absorption products and explore the absorption mechanisms. Deuterated water (D<sub>2</sub>O, purity 99.9%, Aladdin) was added to the samples to obtain the signal lock. Then, the measured data were post-processed using the Bruker TopSpin 3.5 software.

Before the qualitative <sup>13</sup>C NMR tests, the CO<sub>2</sub> was preloaded into single amine solutions to prepare the rich

amine solutions, indicating that the CO<sub>2</sub> loading of each amine solution was over 0.5 mol/mol. During the CO<sub>2</sub> absorption experiments at 313 K, quantitative <sup>13</sup>C NMR tests were performed to measure the concentration of the species in PZ blends with different CO<sub>2</sub> loading at equilibrium.

For the quantitative <sup>13</sup>C NMR tests, the concentration of amine carbamates, bicarbonate, and carbonate can be calculated using the following equations, which were proposed by Holmes et al.<sup>30</sup>

$$\varphi = \frac{S_{\text{AmineCOO}^-}}{S_{\text{HCO}_3^-} + S_{\text{CO}_3^{2-}}} \quad (1)$$

$$[\text{AmineCOO}^-] = \frac{\varphi}{1 + \varphi} [\text{CO}_2]_{\text{loading}} \quad (2)$$

$$[\text{HCO}_3^-] = \frac{168.03 - \delta}{(168.03 - 160.3) \times (1 + \varphi)} [\text{CO}_2]_{\text{loading}} \quad (3)$$

$$[\text{CO}_3^{2-}] = \frac{\delta - 160.3}{(168.03 - 160.3) \times (1 + \varphi)} [\text{CO}_2]_{\text{loading}} \quad (4)$$

where,  $S_{\text{AmineCOO}^-}$ ,  $S_{\text{HCO}_3^-}$ , and  $S_{\text{CO}_3^{2-}}$  present the integral areas of the peaks of amine carbamates, bicarbonate, and carbonate, respectively.  $[\text{AmineCOO}^-]$  is the concentration of MEA-COO<sup>-</sup> or PZCOO<sup>-</sup> in the solutions, in mol/L.  $[\text{CO}_2]_{\text{loading}}$  indicates the total CO<sub>2</sub> loading absorbed in the solutions, in mol/L.  $[\text{HCO}_3^-]$  and  $[\text{CO}_3^{2-}]$  are the concentration of HCO<sub>3</sub><sup>-</sup> and CO<sub>3</sub><sup>2-</sup> ions in solutions, respectively, in mol/L.  $\delta$  presents the chemical shift of HCO<sub>3</sub><sup>-</sup>/CO<sub>3</sub><sup>2-</sup> ions in the solutions. 168.03 and 160.3 are the chemical shifts of solely Na<sub>2</sub>CO<sub>3</sub> and NaHCO<sub>3</sub> solutions measured by the <sup>13</sup>C NMR in our experiments, which is close to the values reported by Jakobsen et al.<sup>31</sup>

#### Parameters Involved in CO<sub>2</sub> Absorption Experiments.

The CO<sub>2</sub> absorption rate ( $r_{\text{ab}}$ , mol CO<sub>2</sub>/L solution/s), defined as the absorbed mole quantities of CO<sub>2</sub> per volume per time, can be predicted by the gas phase based on the difference between the CO<sub>2</sub> concentration of inlet gas and outlet gas, as expressed by the following equation:

$$r_{\text{ab}} = \frac{V_{\text{SFG}}(v_{\text{in}} - v_{\text{out}})}{\left(\frac{60 \text{ s}}{\text{min}}\right)(1 - v_{\text{out}})V_{\text{mole}}V_{\text{solu}}} \quad (5)$$

where  $V_{\text{SFG}}$  is the volumetric flow rate of simulated flue gas, set as the value of 1 L/min;  $V_{\text{mole}}$  is the molar volume of gas at the absorption temperature (L/mol);  $v_{\text{in}}$  (%) and  $v_{\text{out}}$  (ppm) are the volume concentrations of CO<sub>2</sub> in the inlet gas and outlet gas, respectively; and  $V_{\text{solu}}$  presents the volume of amine solutions, in L.

CO<sub>2</sub> loading ( $A_{\text{ab}}$ , mol CO<sub>2</sub>/mol amine) can be calculated from the integral of the CO<sub>2</sub> absorption rate using the following equation, which is defined as the absorbed mole quantities of CO<sub>2</sub> per mole amine.

$$A_{\text{ab}} = \frac{\int_0^t r_{\text{ab}} dt}{n_{\text{amine}}} \quad (6)$$

where  $n_{\text{amine}}$  is the total mole concentration of amines in amine solutions, in mol amine/L solution.

**Computational Methods.** The Gaussian 09 suite of programs<sup>32</sup> was used for the static quantum mechanical (QM) calculations to estimate the enthalpy changes of reactions in

CO<sub>2</sub> absorption at the theory level of B3LYP/6-311++G(d,p). The SMD continuum solvation model proposed by Truhlar et al.<sup>33</sup> with the polarizable continuum model (PCM) approach was used. The vibrational contributions to the free energy were estimated using the harmonic frequency analysis. The calculation method has been proved to be suitable for the study of CO<sub>2</sub>-loaded aqueous amine solutions in simulations conducted by Hwang's group,<sup>23,34</sup> and our predicted results were compared to their results to verify the reliability of our calculations.

Density functional theory (DFT)-based ab initio molecular dynamics (AIMD) simulations were performed using the CPMD code<sup>35,36</sup> coupled with metadynamics sampling using PLUMED plugin<sup>37</sup> to describe the free energy barriers of key elementary reactions. The generalized-gradient approximation exchange-correlation energy functional revised by Perdew, Burke, and Ernzerhof (revPBE<sup>38</sup>) was used in DFT. The kinetic energy cutoff for the plane-wave basis was 40 Rydberg. The timestep was set to 7 au (0.17 fs), and fictitious electrons mass was equal to 700 au. The Nosé–Hoover chain thermostat was used to control the temperature (313 K) of the NVT ensemble. The frequency for the ionic thermostat and the electron thermostat was set to 3000 and 10,000 cm<sup>-1</sup>, respectively. In all CMPD calculations, the mass of all hydrogen atoms was replaced by that of the deuterium, in order to minimize thermal decoupling of modes and ensure adiabaticity.

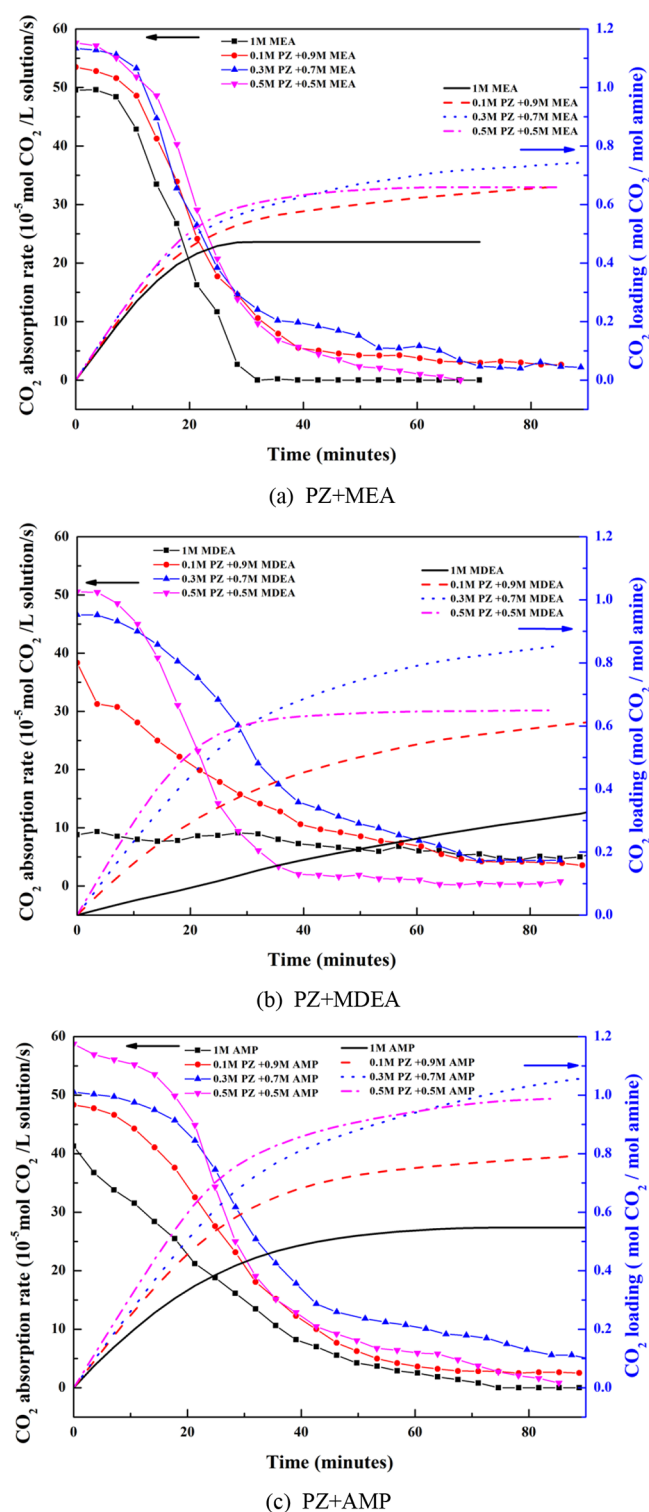
In CPMD-metadynamics simulations, a biased potential (Gaussian-like hill), was dropped at small time intervals in the coordinate space of interest to fill up the free energy surface. The accumulation of these potential hills can construct the free energy surface with respect to the chosen collective variables. We deposited potential hills every 100 timesteps (1 timestep = 0.17 fs) over a trajectory of about 100 ps. Other details of calculations can be found in the [Supporting Information](#).

## RESULTS AND DISCUSSION

**Effect of the Concentration Ratio of PZ Blends on CO<sub>2</sub> Absorption.** The absorption performance of PZ blends was investigated at 313 K, taking the 1 M MEA, 1 M MDEA, and 1 M AMP solutions as the reference solutions. The absorption rates and CO<sub>2</sub> loading profiles of PZ blends with different concentration ratios (PZ/MEA, PZ/MDEA, PZ/AMP) are displayed in [Figure 1](#).

The trend of the CO<sub>2</sub> absorption rate and the CO<sub>2</sub> loading curves of PZ blends with the different concentration ratio had the same varying tendency with the increasing of absorption time. Except for the 1 M MDEA, 0.1 PZ + 0.9 MDEA, and 1 M AMP, the change of the CO<sub>2</sub> absorption rate and the CO<sub>2</sub> loading indicated that the CO<sub>2</sub> absorption process could be divided into three stages: the diffusion control area, the transition area, and the chemical kinetic control area. At the beginning of absorption (the diffusion control area), the CO<sub>2</sub> absorption rate maintained around the highest value, where the reaction rate between CO<sub>2</sub> and PZ blends was larger than the diffusion rate of CO<sub>2</sub> in the gas phase, and thus the absorption rate is controlled by the diffusion rate of CO<sub>2</sub>. Therefore, no major difference among the initial absorption rates of different PZ + MEA or PZ + MDEA or PZ + AMP blends was noticed, which was around the range of 53.5–57.6 or 45.0–50.5 or 48.4–58.7 mol CO<sub>2</sub>/L solution/s, as shown in [Table 1](#). The small increment of the initial absorption rates, showing a positive relationship with the PZ/amine ratio, can be explained





**Figure 1.** Absorption rates and  $\text{CO}_2$  loading profiles of PZ + MEA (a), PZ + MDEA (b), and PZ + AMP (c) solutions.

that the PZ has a positive effect on the  $\text{CO}_2$  diffusion from the gas phase to the gas–liquid interface as the surfactant. With the increase of  $\text{CO}_2$  loading in PZ blends, the reaction rate between  $\text{CO}_2$  and amine solutions decreased, and the absorption process moved to the transition area. At this stage, the absorption rate was controlled by both the diffusion rate and reaction rate, and the absorption rate cut down to more than 60% quickly with the increment of time (from 10 to

30 min). After that, the absorption process moved to the chemical kinetic control area, where the absorption rate decreased gently and approached zero as the great consumption of amines.

For the 0.1 PZ + 0.9 MDEA and 1 M AMP, because the reaction rate between  $\text{CO}_2$  and aqueous amines was lower than the  $\text{CO}_2$  diffusion rate at the beginning of the absorption, the absorption process stepped directly into the transition area followed by the chemical kinetic control area. For the 1 M MDEA, the absorption process was entirely controlled by the chemical kinetic of the reaction between  $\text{CO}_2$  and aqueous MDEA, which was related to the low reaction activity of MDEA.

The 1 M MEA reached the saturation of absorption within 30 min, while the 1 M MDEA did not reach the saturation in 90 min. It is easy to understand that the reaction rate of the bicarbonate formation in the MDEA solution is much slower compared to that of the carbamate formation in the MEA solution. Similarly, the  $\text{CO}_2$  absorption rate of PZ + MEA blends was faster than that of PZ + MDEA blends, and the  $\text{CO}_2$  absorption rate of PZ + AMP blends fell somewhere in between.

The  $\text{CO}_2$  loading of each PZ blend and their increments in 80 min compared to the pure MEA/MDEA/AMP solution are also categorized in Table 1. The  $\text{CO}_2$  loadings of all PZ blends increased properly with the increasing addition amount of PZ and reached the optimum at around 0.3 mol/L, and then the promoting effect started to decrease with extra PZ addition. Specially, the  $\text{CO}_2$  loadings of 0.3 M PZ + 0.7 M MEA, 0.3 M PZ + 0.7 M MDEA, and 0.3 M PZ + 0.7 M AMP at 80 min were 0.73, 0.85, and 1.043 mol/mol, respectively, which were 56, 179, and 90.6% higher than those of 1 M MEA, 1 M MDEA, and 1 M AMP. This phenomenon may be related to the high viscosity of PZ blends with high PZ concentration, which played a negative role in the diffusion of absorption products from the gas–liquid phase to the bulk solution.

It is well known that PZ has high reaction kinetics with  $\text{CO}_2$  than MEA, MDEA, and AMP. Thus, with the increase of the PZ/amine ratio, the absorption rate of PZ blends was supposed to increase. However, our experimental results pointed out that the absorption of  $\text{CO}_2$  in PZ blends was not the simple combination of PZ- $\text{CO}_2$  reactions and amine- $\text{CO}_2$  reactions; the intermolecular effects should not be ignored, which will be discussed further in our next experiments and calculations. The optimized ratio of PZ blends was 0.3 M PZ + 0.7 M MEA(MDEA/AMP) in our experiments, just taking the absorption performance into account. The optimized PZ blends needed to be comprehensively evaluated in dynamic absorption–desorption to improve the total absorption–desorption efficiencies<sup>39</sup> further.

**Liquid Phase Composition of PZ-Amine- $\text{CO}_2$ - $\text{H}_2\text{O}$  Systems.** The qualitative  $^{13}\text{C}$  NMR spectroscopy was used to explore the reactions of  $\text{CO}_2$  with mixed PZ + MEA, PZ + MDEA, and PZ + AMP solutions. The  $^{13}\text{C}$  NMR stack plots for fresh PZ + rich MEA with rich PZ + fresh MEA, fresh PZ + rich MDEA with rich PZ + fresh MDEA, and fresh PZ + rich AMP with rich PZ + fresh AMP are shown in Figure 2a–c, respectively. The corresponding molecular structures with C atom assignments and chemical shift ranges are given in Table 2.

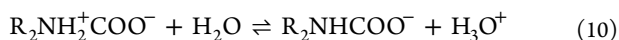
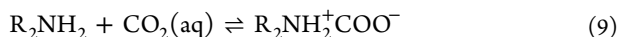
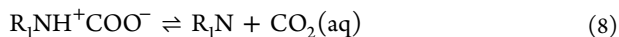
Compared to the  $^{13}\text{C}$  NMR spectrum of fresh PZ + MEA solutions (as shown in Figure S1 in the Supporting Information), the additional resonances in all PZ blends

**Table 1. Initial Absorption Rate, CO<sub>2</sub> Loading, and Increment of CO<sub>2</sub> Loading of Amine Solutions**

amine solutions	initial absorption rate (mol CO <sub>2</sub> /L solution/s)	CO <sub>2</sub> loading (mol CO <sub>2</sub> /mol amine)	increment of CO <sub>2</sub> loading
1 M MEA	49.51	0.472	
0.1 M PZ + 0.9 M MEA	53.45	0.657	39.2%
0.2 M PZ + 0.8 M MEA	54.24	0.667	41.3%
0.3 M PZ + 0.7 M MEA	56.69	0.735	55.7%
0.4 M PZ + 0.6 M MEA	57.56	0.554	17.4%
0.5 M PZ + 0.5 M MEA	57.61	0.659	39.6%
1 M MDEA	8.78	0.303	
0.1 M PZ + 0.9 M MDEA	38.32	0.596	96.7%
0.2 M PZ + 0.8 M MDEA	44.94	0.674	122%
0.3 M PZ + 0.7 M MDEA	46.61	0.846	179%
0.4 M PZ + 0.6 M MDEA	49.99	0.645	113%
0.5 M PZ + 0.5 M MDEA	50.54	0.649	114%
1 M AMP	41.24	0.547	
0.1 M PZ + 0.9 M AMP	48.36	0.784	43.3%
0.2 M PZ + 0.8 M AMP	49.11	0.810	48.1%
0.3 M PZ + 0.7 M AMP	50.51	1.043	90.6%
0.4 M PZ + 0.6 M AMP	54.12	0.981	79.4%
0.5 M PZ + 0.5 M AMP	58.73	0.986	80.3%

emerged around 164.0 ppm, which corresponded to the carbamate carboxyl carbon (MEACOO<sup>−</sup>, PZCOO<sup>−</sup>, or AMPCOO<sup>−</sup>). The small differences in the chemical shifts for the C atom with the same tagged symbols should be due to the differences in the molecules' protonation and pH value in different PZ blends.<sup>40</sup>

The PZCOO<sup>−</sup> peaks (P1'/P2/P3) and MEACOO<sup>−</sup> peaks (M1'/M2'/M3) appeared in both 1 M fresh PZ + 1 M rich MEA and 1 M rich PZ + 1 M fresh MEA solutions, as shown in Figure 2a, which indicated the conversion between PZCOO<sup>−</sup> and MEACOO<sup>−</sup> in PZ + MEA solutions. We assumed that the conversion between PZCOO<sup>−</sup> and MEACOO<sup>−</sup> was accomplished through the reaction pathways, including the protonation of carbamate, CO<sub>2</sub> release, another zwitterion formation, and the deprotonation of zwitterion to form another carbamate, as demonstrated in the following equations.



Moreover, the peak of PZCOO<sup>−</sup> (P3) had a lower signal intensity than the peak of MEACOO<sup>−</sup> (M3) in both 1 M fresh PZ + 1 M rich MEA (154 < 399) and 1 M rich PZ + 1 M fresh MEA (116 < 212) solutions, which verified that under dynamic equilibrium, the concentration of MEACOO<sup>−</sup> was higher than that of PZCOO<sup>−</sup> in PZ + MEA solutions. This was consistent with the NMR results from Ciftja et al.,<sup>41</sup> indicating that MEACOO<sup>−</sup> had the higher stability than PZCOO<sup>−</sup>.

Compared to the <sup>13</sup>C NMR spectrum of fresh PZ + MDEA solutions, the peak of PZCOO<sup>−</sup> can be found in the 1 M fresh PZ + 1 M rich MDEA, indicating the occurrence of conversion from bicarbonate to PZCOO<sup>−</sup> in the PZ + MDEA solution. A similar phenomenon can also be found in the PZ + AMP solution.

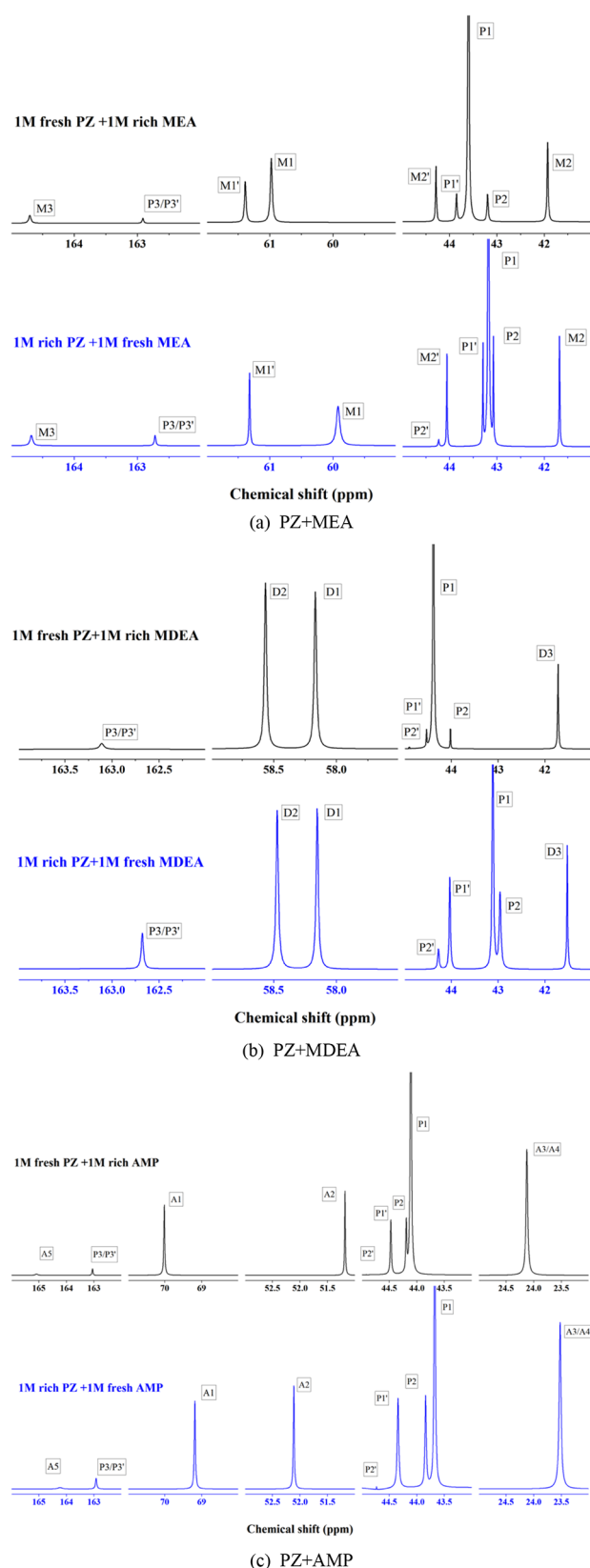
Combining the experimental results and qualitative NMR results, we can assume that PZ can be considered to be the

“absorption activator” in the PZ blends, and the improvement of the absorption performance was significant even with a bit addition of PZ. This can be explained by the proposed “shuttle mechanism”<sup>13</sup> that the excessive other amines helped to release free PZ out of the “carbamate-ammonium salt” via “conversion between absorption products” and “protonated amine” via “proton transfer”.<sup>42</sup>

**The Concentration of Absorption Products in PZ Blends with the Change of CO<sub>2</sub> Loading.** The concentrations of the carbamates, protonated amines, and bicarbonate in PZ blends as a function of CO<sub>2</sub> loading, calculated from the quantitative <sup>13</sup>C NMR analysis, are presented in Figure 3. The total concentration of amines of PZ blends was kept at 1 mol/L, with the constant concentration ratio of PZ and MEA/MDEA/AMP at 3:7. The method developed by Ciftja et al.<sup>16</sup> was used to distinguish amine from protonated amine and carbonate from bicarbonate, which cannot be observed directly due to the fast exchanging of protons.<sup>43,44</sup> Considering that the COO<sup>−</sup>PZCOO<sup>−</sup> is far less thermodynamically relative to PZCOO<sup>−</sup><sup>45</sup> and its peak (P2') is much lower than the PZCOO<sup>−</sup> peak (P2) (as shown in Figure S2 in the Supporting Information), the concentration of COO<sup>−</sup>PZCOO<sup>−</sup> is ignored in each PZ blend.

As shown in Figure 3a, the concentration of free MEA decreased with the increasing of the CO<sub>2</sub> loading, as the MEA was converted to the MEAH<sup>+</sup> and the MEACOO<sup>−</sup>. The concentration of MEAH<sup>+</sup> increased less steeply under low CO<sub>2</sub> loading and slightly more steeply when the CO<sub>2</sub> loading was higher after the exhaustion of PZ. In the beginning, both the free MEA and free PZ played the role of a proton acceptor, but there was only one proton acceptor (MEA) in the rich CO<sub>2</sub> loading stage after the complete consumption of free PZ. It can be noted that PZ was more favorable as the proton acceptor, owing to its high pK<sub>a</sub> and high availability (two basic sites) for proton access.

In the PZ + MEA solution, the concentration of MEACOO<sup>−</sup> was 2.5–5 times of the concentration of PZCOO<sup>−</sup> when the CO<sub>2</sub> loading was lower than 0.45 mol CO<sub>2</sub> mol/mol. The multiple was larger than the ratio of MEA initial concentration to that of PZ (2.33). This phenomenon indicated that at this

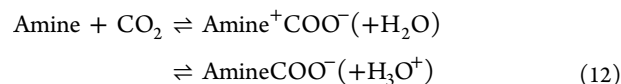
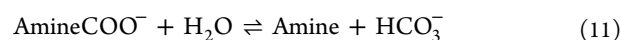


**Figure 2.**  $^{13}\text{C}$  NMR spectra of PZ + MEA, PZ + MDEA, and PZ + AMP solutions for the qualitative identification of absorption species.

stage,  $\text{MEACOO}^-$  appeared before  $\text{PZCOO}^-$ , which was consistent with the experimental results of Zhang et al.<sup>4</sup> It is owing to the conversion between  $\text{PZCOO}^-$  and  $\text{MEACOO}^-$

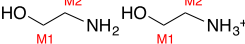

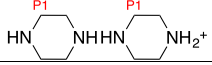
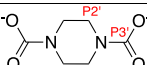
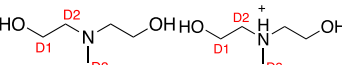
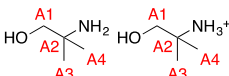
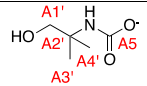
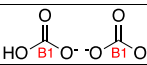
and the high thermal stability of  $\text{MEACOO}^-$ , as also mentioned in *Liquid Phase Composition of PZ-Amine-Carbon Dioxide-Water Systems*. Specifically, in the PZ + MEA solution, PZ and MEA may compete for  $\text{CO}_2$  absorption to form carbamates, and the reaction between PZ and  $\text{CO}_2$  shows a higher reaction rate. Then, the carbamate formation can be followed by a further conversion between  $\text{PZCOO}^-$  and  $\text{MEACOO}^-$ , in which the amine carbamates break down to reform the solvated  $\text{CO}_2$  and fresh amine, as shown in eqs 6–10. This leads to the equilibration of carbamates since the reactions are symmetrical and reversible, and this assumption is in agreement with that in Ballard et al.'s study<sup>13</sup> and the “shuttle mechanism” first proposed by Astarita et al.<sup>46</sup>

The species distribution of  $\text{MEA-H}_2\text{O-CO}_2$  in the PZ + MEA blend showed the typical behavior of primary amines;<sup>47</sup> these trends of absorption products were consistent with that in the single MEA<sup>48</sup> and MEA + DEAB solutions.<sup>49</sup> When the  $\text{CO}_2$  loading was lower than 0.45 mol/mol, a large part of  $\text{CO}_2$  was chemically bound in  $\text{MEACOO}^-$  and a small part of  $\text{CO}_2$  was formed in  $\text{PZCOO}^-$ ; thereby, the concentration of  $\text{MEACOO}^-$  or  $\text{PZCOO}^-$  showed linear change with the  $\text{CO}_2$  loading. During this stage, the concentration of  $\text{MEA}^+\text{H}^+$  and  $\text{PZH}^+$  also increased. When the  $\text{CO}_2$  loading was larger than 0.45 mol/mol, the mole concentration of free MEA has dropped down to almost zero, which means that the MEA was either converted to  $\text{MEACOO}^-$  or protonated to  $\text{MEA}^+\text{H}^+$ . With the further increase of  $\text{CO}_2$  loading, the concentration of  $\text{MEA}^+\text{H}^+$  increased accompanied by the expense of  $\text{MEACOO}^-$ , and thus the decline of the  $\text{MEACOO}^-$  concentration can be found. This phenomenon indicated the occurrence of the hydrolysis reaction of the  $\text{MEACOO}^-$  (eq 11) or the break-down reaction of  $\text{MEACOO}^-$  (reverse reaction in eq 12) releasing  $\text{CO}_2$ , where  $\text{CO}_2$  released from  $\text{MEACOO}^-$  to form bicarbonate. Therefore, the bicarbonate started to form and its concentration increased, while the concentration of  $\text{CO}_3^{2-}$  was limited and close to zero throughout due to its low solubility in alkaline solution. The same change of  $\text{PZCOO}^-$  concentration and  $\text{PZH}^+$  concentration can also be found when the  $\text{CO}_2$  loading was around 0.6 mol/mol.



Some researchers hold the idea that the  $\text{HCO}_3^-$  was mainly released out of amine carbamates via the carbamate hydrolysis reaction,<sup>50</sup> as shown in eq 11. Meanwhile, both Said et al.'s<sup>51</sup> and Davran-Candan's<sup>52</sup> simulation results predicted that the activation barriers for the hydrolysis conversion of carbamates were all higher than 36 kcal/mol, while the activation barrier for bicarbonate formation through the base-catalyzed hydration mechanism (eq 13) was around 8 kcal/mol,<sup>52,53</sup> indicating that the carbamate hydrolysis reaction was extremely kinetically unfavorable. Thus, the bicarbonate observed in the PZ + MEA solution under the high  $\text{CO}_2$  loading was formed through the base-catalyzed hydration mechanism after the break-down of  $\text{MEACOO}^-$  or  $\text{PZCOO}^-$  (reverse reaction in eq 12), which was along with the phenomena in MEA solution.<sup>52</sup> The concentration of  $\text{H}^+$  ions increased with the increasing  $\text{CO}_2$  loading, and the equilibrium (eq 10) was

Table 2. Chemical Shifts of the Corresponding C Atoms of Absorption Products in Rich PZ Blends

Signal symbol	Chemical shift (ppm)	Assignment
M1	59.93-60.97	
M2	41.67-41.92	
M1'	61.31-61.38	
M2'	43.07-43.20	
M3	164.67-164.71	
P1	43.18-43.60	
P1'	43.29-44.03	
P2	42.95-43.19	
P3	162.67-163.11	
P2'	44.17-44.28	
P3'	162.67-163.11	
D1	58.15-58.17	
D2	58.56-58.47	
D3	41.52-41.72	
A1	70.15-69.00	
A2	52.22-51.11	
A3/A4	24.34-23.22	
A5	165.16-164.06	
B1	161.2-162	

therefore shifted to the left toward zwitterion and then released amine and  $\text{CO}_2$ . Thus, the higher  $\text{CO}_2$  absorption is suggested to lead to the destabilization of carbamate and ultimately to promote the conversion from carbamate to bicarbonate.

As depicted in Figure 3b, in the initial stage ( $\text{CO}_2$  loading < 0.1 mol/mol) of the PZ-MDEA- $\text{CO}_2$ - $\text{H}_2\text{O}$  system,  $\text{PZCOO}^-$  was the only anion of  $\text{CO}_2$  absorption, where  $\text{CO}_2$  mainly reacted with PZ in the PZ + MDEA solution. Even some MDEA reacted with  $\text{CO}_2$  forming  $\text{HCO}_3^-$ , and the  $\text{HCO}_3^-$  would ultimately convert to  $\text{PZCOO}^-$  with the existence of free PZ as the low thermal stability of  $\text{HCO}_3^-$ . Therefore, the initial absorption rates of PZ + MDEA solutions did not include the  $\text{HCO}_3^-$  formation reactions. When the  $\text{CO}_2$  loading reached 0.3 mol  $\text{CO}_2$ /mol amine, the bicarbonate started to form due to the exhaustion of PZ. This is because PZ shows a higher reaction activity with  $\text{CO}_2$  compared to MDEA, and hence  $\text{CO}_2$  reacts with PZ preferentially.

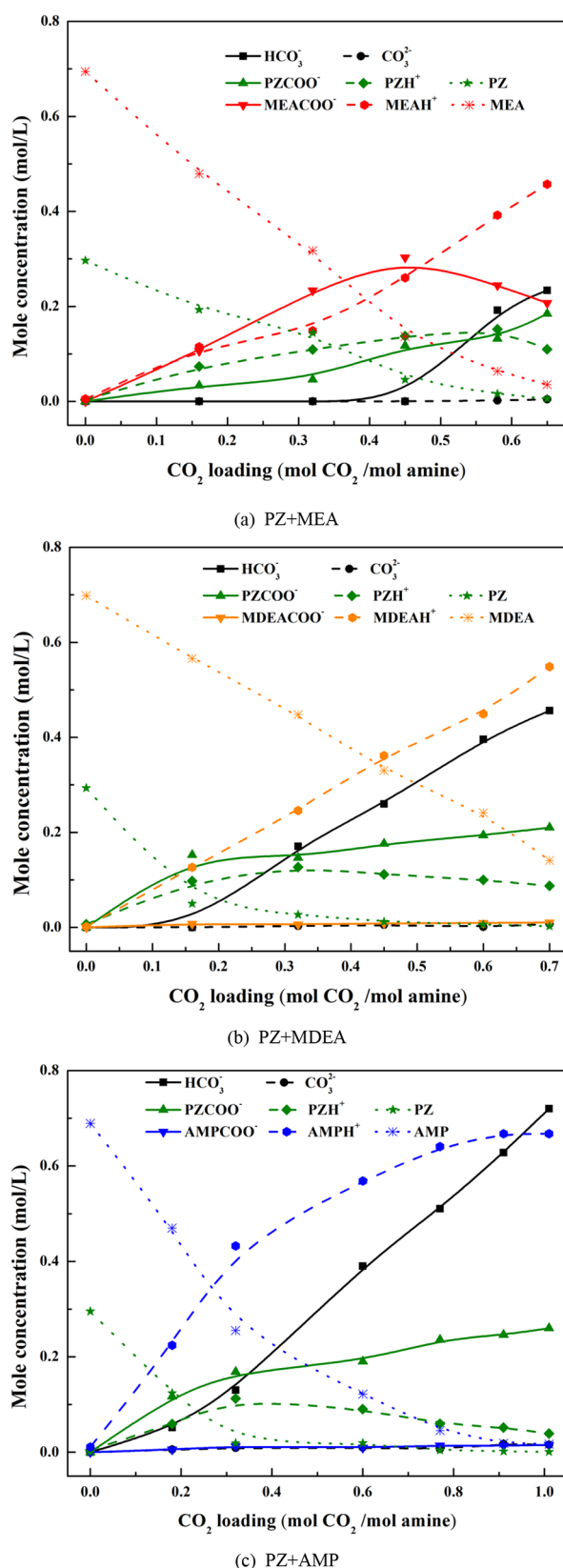
With the increasing of the  $\text{CO}_2$  loading, the absorption process in the PZ + MDEA blend can be divided into three stages based on the formation of different products. In the first stage, when the  $\text{CO}_2$  loading was smaller than 0.3 mol  $\text{CO}_2$ /mol amine, the  $\text{PZCOO}^-$  was the only product, without the existence of  $\text{HCO}_3^-/\text{CO}_3^{2-}$ . Or, a small amount of  $\text{HCO}_3^-/\text{CO}_3^{2-}$  was generated at the very beginning, acting as the intermediate products and converting to  $\text{PZCOO}^-$  as the stronger ability of PZ. In the second stage, the absorption products include both  $\text{PZCOO}^-$  and  $\text{HCO}_3^-$ , owing to the limitation of fresh PZ in the solution. During this stage, the competitive relationship between PZ and MDEA for  $\text{CO}_2$  absorption was expressed. When the  $\text{CO}_2$  loading was higher than 0.32 mol  $\text{CO}_2$ /mol amine, it turned to be the third stage, during which the concentration of  $\text{PZH}^+$  decreased with the

increasing of the  $\text{CO}_2$  loading. This was because the proton was transferred from  $\text{PZH}^+$  to  $\text{MDEAH}^+$ , releasing PZ to capture  $\text{CO}_2$ .

As shown in Figure 3c, unlike the change tendency of  $\text{MEAH}^+$  concentration, the concentration of  $\text{AMP}^+$  increased steeply in the beginning and less steeply at higher  $\text{CO}_2$  loading as the exhaustion of AMP. Thus, the relationship of the favorability for the proton attraction was in the order of:  $\text{AMP} > \text{PZ} > \text{MEA} > \text{MDEA}$ . The minimum  $\text{CO}_2$  loading in which bicarbonate was detected in the PZ + AMP solution was smaller than that in the PZ + MDEA solution, as shown in Figure 3b,c. This was related to the competition between PZ and AMP (PZ and MDEA) interacting with  $\text{CO}_2$ , and AMP showed a higher rate of  $\text{HCO}_3^-$  formation than MDEA. Therefore, combined with the above discussion, the formation of  $\text{HCO}_3^-$  in the PZ + MEA solution was a bit different from that in the PZ + AMP or PZ + MDEA solution, which was related to the carbamate breakdown and the generation of bicarbonate.

Comparing the concentration of  $\text{PZCOO}^-$  and  $\text{PZH}^+$  in PZ + MDEA and PZ + AMP solutions, it can be noted that except for the effect of based-catalysis for bicarbonate formation, both MDEA and AMP can also play the role of a Brønsted base or proton acceptor in the reactions between PZ and  $\text{CO}_2$ , releasing more free PZ molecules to attack  $\text{CO}_2$  and accelerating the absorption rate. The concentration ratio of  $\text{PZCOO}^-$  and  $\text{HCO}_3^-$  under the  $\text{CO}_2$  loading around 0.6 mol/mol in PZ + MDEA and PZ + AMP solution was 0.489 and 0.488, respectively, which was higher than the hypothetical ratio of  $\text{PZCOO}^-$  and  $\text{HCO}_3^-$  (0.214) based on the simple combination of 0.3 M PZ solution and 0.7 M MDEA/AMP solution. This result also indicated that MDEA/AMP played



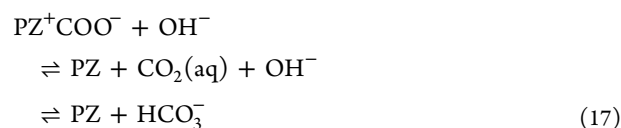


**Figure 3.** Liquid phase speciation in PZ-amine- $\text{CO}_2$ - $\text{H}_2\text{O}$  systems: (a) 0.3 M PZ + 0.7 M MEA; (b) 0.3 M PZ + 0.7 M MDEA; (c) 0.3 M PZ + 0.7 M AMP.

the role of the proton acceptor to release free PZ to react with  $\text{CO}_2$ .

Comparing the concentration change of products ions in PZ blends, the PZ + MEA and PZ + MDEA solutions are two kinds of extremes. To be more specific, in the PZ + MEA solutions, PZ and MEA compete with each other to react with  $\text{CO}_2$ , while in PZ + MDEA solutions, MDEA almost plays the role of the proton acceptors, and the condition of PZ + AMP solution is somewhere in between.

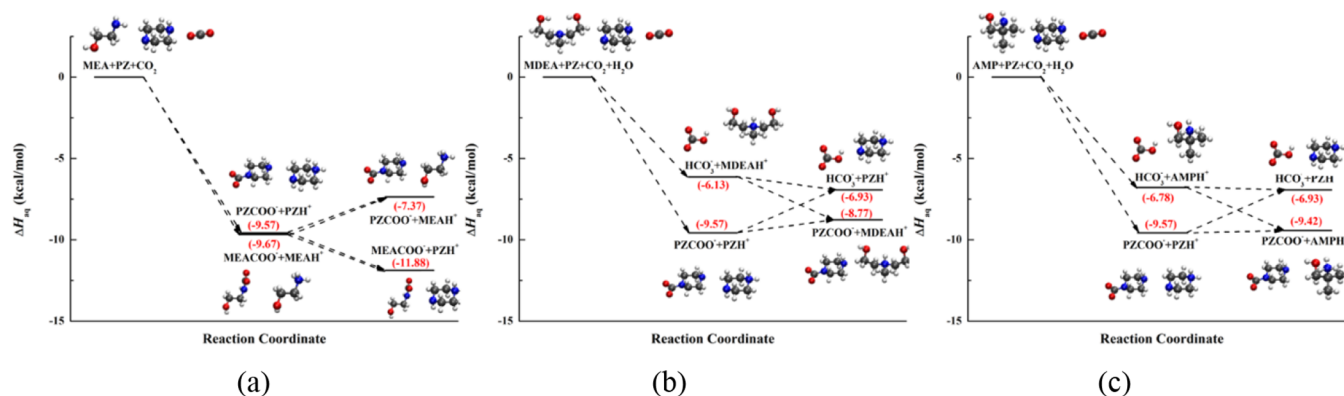
Moreover, the reactions between  $\text{CO}_2$  and PZ + amines were not the simple combinations of reactions between PZ with  $\text{CO}_2$  and reactions between amines with  $\text{CO}_2$ . Take the PZ + AMP solution as an example, the addition of PZ will help to split the energy barrier of the difficult one-step  $\text{HCO}_3^-$  formation (eq 14) into two less difficult steps (a)  $\text{PZCOO}^-$  formation (eqs 15 and 16) and then (b)  $\text{HCO}_3^-$  formation from the combination of  $\text{OH}^-$  and  $\text{CO}_2$  (aq) (eq 17). It is much easier for  $\text{CO}_2$  to be attacked by PZ initially than the hydration with  $\text{H}_2\text{O}$  under basic catalysis of AMP, and thus the overall absorption rate is greatly accelerated in PZ blends. Therefore, the PZ plays two roles in PZ blends; first, it itself reacts with  $\text{CO}_2$  forming  $\text{PZCOO}^-$  with a high absorption rate; second, it plays the role of being a “shuttle”, which alters the reaction pathway and accelerates the reaction rate of  $\text{HCO}_3^-$  formation but does not change the thermodynamics nor the absorption products.



From Figure 3a–c, it can also be found that under the  $\text{CO}_2$  loading of around 0.6 mol/mol, the final concentration of  $\text{PZCOO}^-$  and  $\text{MEACOO}^-$  in the PZ + MEA solution was 0.132 and 0.244 mol/L, and the final concentration of  $\text{PZCOO}^-$  in the PZ + MDEA solution and PZ + AMP solution was 0.194 and 0.190 mol/L, respectively. Taking the high stability of  $\text{PZCOO}^-$  and  $\text{MEACOO}^-$  into account, more energy will be needed for the regeneration of the PZ + MEA solution compared to the PZ + MDEA/PZ + AMP solution, with less difference of the absorption performance between these two PZ blends (see details in Figure S3 in the Supporting Information).

**Absorption–Desorption Mechanisms of  $\text{CO}_2$  in PZ Blends.** Based on our assumption of the conversion between absorption products in PZ blends as mentioned above, the proposed reaction routes in PZ + MEA, PZ + MDEA, and PZ + AMP solutions are illustrated in Figure 4, along with predicted changes in enthalpy using static QM calculations. The enthalpies and free energies of all reactants and products are shown in Table S1 in the Supporting Information. The enthalpy change of  $\text{MEACOO}^-$  formation ( $2\text{MEA} + \text{CO}_2 \rightarrow \text{MEACOO}^- + \text{MEAH}^+$ ) was consistent with the values predicted by Hwang et al.<sup>23</sup> and Yoon et al.,<sup>34</sup> and the predicted pKa of PZ/MEA/AMP/MDEA was also very close to the measured pKa value from previous studies, as shown in Table S2 in the Supporting Information. PZ and MEA may react with  $\text{CO}_2$  to form carbamate ( $\text{PZCOO}^-$  and  $\text{MEACOO}^-$ ) and protonated amine ( $\text{PZH}^+$  and  $\text{MEAH}^+$ ),





**Figure 4.** Proposed reaction route of the CO<sub>2</sub> absorption in aqueous (a) PZ + MEA, (b) PZ + MDEA, and (c) PZ + AMP solutions together with predicted enthalpy changes ( $\Delta H_{aq}$ ) with respect to isolated PZ+ amines and CO<sub>2</sub> using static QM calculations.

and their products showed similar thermodynamic stability with the small difference of the enthalpy change (0.1 kcal/mol). The reaction of proton transfer from MEAH<sup>+</sup> to PZ was more exothermic with the enthalpy change of  $-2.21$  kcal/mol compared to that from MDEAH<sup>+</sup> to PZ ( $-0.8$  kcal/mol) and from AMPH<sup>+</sup> to PZ ( $-0.15$  kcal/mol). This result is related to the basicity of amine, which is in the relation of  $\text{pKa}(\text{PZ}) = 9.71 > \text{pKa}(\text{AMP}) = 9.68 > \text{pKa}(\text{MEA}) = 9.44^{54} > \text{pKa}(\text{MDEA}) = 8.76^{55}$ . The enthalpy change of the conversion reaction from PZCOO<sup>-</sup> to MEACOO<sup>-</sup> was predicted to be  $-2.30$  kcal/mol, indicating that the formation of MEACOO<sup>-</sup> in PZ + MEA was more thermodynamic favorable. Thus, from the thermodynamic point of view, the concentration ratio of MEACOO<sup>-</sup> and PZCOO<sup>-</sup> would be higher than the initial concentration ratio of MEA and PZ, and also the concentration ratio of PZH<sup>+</sup> and MEAH<sup>+</sup> would be higher than the initial concentration ratio of PZ and MEA, which was coincident with that of experiments as shown in Figure 3a.

Comparing the enthalpy change of bicarbonate formation by MDEA-catalyzed hydration and AMP-catalyzed hydration in Figure 4b,c, the latter was more exothermic. Thus, the formation of bicarbonate in PZ-AMP was more thermodynamically favorable than that in PZ-MDEA, and this was also in accordance with the experimental results that the minimum CO<sub>2</sub> loading in which bicarbonate was detected in PZ + AMP solution was smaller than that in PZ + MDEA. Our static QM calculations predicted that the conversion from bicarbonate to PZCOO<sup>-</sup> in PZ + MDEA or PZ + AMP was an endothermic reaction with the enthalpy change of  $2.64$  kcal/mol, indicating that the formation of PZCOO<sup>-</sup> showed higher thermodynamic favorability. However, at dynamic equilibrium, we can expect that bicarbonate formation would become significant at high CO<sub>2</sub> loading, when the concentration of PZCOO<sup>-</sup> is much higher than that of free PZ.

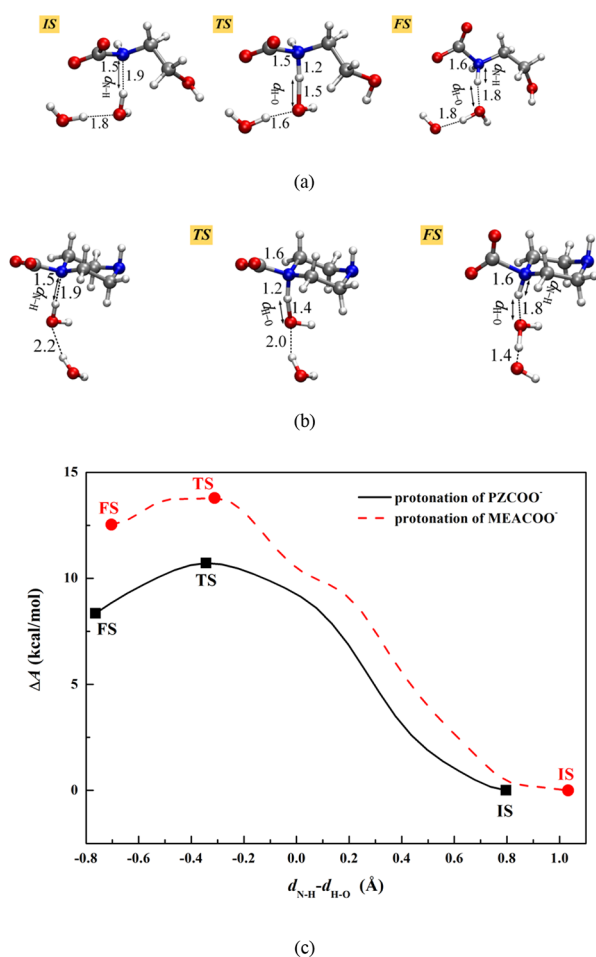
Next, we examined the energy barrier of the key elementary reaction for the conversion of carbamates to explore the reaction kinetics of the conversion between absorption products. As mentioned above, the conversion between absorption products may go through four elementary reactions, including the carbamate breakdown, CO<sub>2</sub> release, zwitterion formation, and deprotonation of zwitterion (or formation of bicarbonate by amine-catalyzed hydration in PZ + AMP/PZ + MDEA). Among them, the carbamate breakdown is the critical and initial step due to the high thermodynamic stability of carbamates, which contains the protonation of carbamate to

form zwitterion and the deprotonation of protonated amine to form free amine.

CPMD-metadynamics simulations at 313 K were performed to evaluate the reaction pathways and free-energy barrier for the protonation of PZCOO<sup>-</sup> and MEACOO<sup>-</sup> in aqueous PZ blends, and the simulation details can be found in the Supporting Information. In the protonation of carbamate, any available proton is attracted by the N atom of carbamate; then, the sp<sup>2</sup> hybridization of N atom (bonded with C atoms) converts to sp<sup>3</sup> hybridization, and the de-localized N–COO– conjugation is weakened at the same time<sup>56</sup> followed by the stretch of N–C bond in preparation for CO<sub>2</sub> release. The detailed molecular structures of the initial state, the transition state, and the final state of the protonation of MEACOO<sup>-</sup> and PZCOO<sup>-</sup> are shown in Figure 5a,b, respectively. The whole proton transfer process through the hydrogen network around the carbamate and protonated amine are shown in Figure S4 in the Supporting Information, taking the protonation of PZCOO<sup>-</sup> as an example.

The free-energy barrier for the protonation of PZCOO<sup>-</sup> and MEACOO<sup>-</sup> was predicted to be  $10.72$  and  $13.79$  kcal/mol, respectively. The lower energy barrier for the protonation of PZCOO<sup>-</sup> indicated that the reaction was more kinetically favorable than the protonation of MEACOO<sup>-</sup>, which may be related to the higher thermal stability of MEACOO<sup>-</sup> as calculated from our static QM calculations. Meanwhile, the difference of these two free-energy barriers was not large, and the value was not a huge amount, indicating that both of the protonation of PZCOO<sup>-</sup> and MEACOO<sup>-</sup> can occur to some degree at 313 K. Compared to the free energy requirement of the deprotonation of MEAH<sup>+</sup>, which was about  $17.54$  kcal/mol (at 25 °C) calculated from the experimental deprotonation constant  $K_a$ , the free energy barrier for protonation of MEACOO<sup>-</sup> was a bit smaller. It can be assumed that the protonation of MEACOO<sup>-</sup> was considered to first occur with the generation of free OH<sup>-</sup> ions, which then help the subsequent deprotonation of MEAH<sup>+</sup>. These simulation results were in accordance with the experimental results that the conversion between absorption products was confirmed and the breakdown of PZCOO<sup>-</sup> was more kinetically favorable.

Indeed, the carbamate breakdown is not easy at room temperature, as the key elementary step (carbamate attracts proton to form zwitterion) requires a large number of free protons and heat. At room temperature, the heat is not enough to overcome the energy barrier, and also the availability of



**Figure 5.** Free energy profile for the protonation of carbamate reaction ( $\text{MEACOO}^- + \text{H}_2\text{O} \rightarrow \text{MEA}^+\text{COO}^- + \text{OH}^-$ ,  $\text{PZCOO}^- + \text{H}_2\text{O} \rightarrow \text{PZ}^+\text{COO}^- + \text{OH}^-$ ) predicted from metadynamics-biased CPMD simulations at 313 K. The system contains  $38\text{H}_2\text{O}$ ,  $1\text{MEACOO}^-$  ( $\text{PZCOO}^-$ ), and  $1\text{MEA}^+\text{H}^+$  ( $1\text{PZ}^+\text{H}^+$ ) molecules in a cubic periodic box with a side length of 11.02 Å (11.31 Å). The collective variable (CV) employed here was the difference between the distance of C in carbamate and H in the nearest  $\text{H}_2\text{O}$  neighbor ( $d_{\text{N-H}}$ ) and the distance of the H and O in the nearest  $\text{H}_2\text{O}$  ( $d_{\text{O-H}}$ ). The positions of initial states, transition states, and final states for both protonation of  $\text{MEACOO}^-$  and  $\text{PZCOO}^-$  were also indicated in (a, b), respectively. The blue, gray, red, and white balls represent N, C, O, and H atoms, respectively.

many free protons is limited as free protons are bonded to amines.<sup>57</sup>

## CONCLUSIONS

In this study, the results from lab-scaled experimental research on  $\text{CO}_2$  absorption using differently concentrated PZ + MEA, PZ + MDEA, and PZ + AMP blends were presented and discussed. The amine concentration of PZ blends was varied, and the total concentration of amine was fixed at 1 M to show the effect of concentration ratio and the influence of amine components on  $\text{CO}_2$  absorption rate and capacity. The addition of PZ was effective in the acceleration of  $\text{CO}_2$  absorption in the MEA/MDEA/AMP solutions. The improvement of the absorption rates in the MDEA solutions was more obvious than that in MEA solutions, but the  $\text{CO}_2$  loadings of PZ + MEA blends were improved to more than 0.5 mol  $\text{CO}_2$ /mol amine.

The ion speciation analyses were then performed in conjunction with the quantitative analysis of product concentration with the change of  $\text{CO}_2$  loading to enable the estimation of possible reaction pathways underlying  $\text{CO}_2$  absorption by PZ blends. The conversion between absorption products was approved by the qualitative  $^{13}\text{C}$  NMR analysis, and the fundamental mechanism was studied under different  $\text{CO}_2$  loading in PZ blends, which contained the processes of carbamate break down,  $\text{CO}_2$  release, zwitterion formation, and deprotonation of zwitterion (or bicarbonate formation in one step). The improvement of the absorption performance was due to the conversion between absorption products, which helped to release free PZ from “carbamate-ammonium salt”.

Using static QM calculations, we first confirmed the thermodynamic stability of absorption products in PZ blends. Then, the free-energy barriers for the deprotonation of carbamates to form zwitterion, which was the key elementary reaction in the conversion between absorption products, were predicted using metadynamics-biased CPMD simulations at 313 K. Our simulation results were in line with our experimental phenomenon, indicating that the conversion between absorption products and the breakdown of  $\text{PZCOO}^-$  were more kinetically favorable.

Our combined experimental and computational study highlights that the blended PZ with amines is a useful technique for the improvement of the absorption rate, absorption capacity, and amine regeneration, which is largely governed by the conversion between absorption products. The improved understanding may aid in efforts to enhance the “shuttle mechanism” of PZ and develop more promising PZ blends for  $\text{CO}_2$  capture.

## ASSOCIATED CONTENT

### Supporting Information

The Supporting Information is available free of charge at <https://pubs.acs.org/doi/10.1021/acs.iecr.1c04123>.

Additional computational details;  $^{13}\text{C}$  NMR spectra of free PZ + MEA, PZ + MDEA, and PZ + AMP solutions;  $^{13}\text{C}$  NMR spectra of rich PZ + MEA +  $\text{CO}_2$ , PZ + MDEA +  $\text{CO}_2$ , and PZ + AMP +  $\text{CO}_2$  systems; absorption performance comparison of the PZ + MEA, PZ + MDEA, and PZ + AMP solutions; enthalpies and free energies (in kcal/mol) from static QM calculations; predicted pKa (298.15 K) of MEA, PZ, AMP, and MDEA calculated from the Gibbs free energy change of amine protonation reaction using the static QM calculations (PDF)

## AUTHOR INFORMATION

### Corresponding Author

Na Li – State Key Laboratory of Multiphase Flow in Power Engineering, Xi'an Jiaotong University, Xi'an 710049, China; [orcid.org/0000-0002-7975-4862](https://orcid.org/0000-0002-7975-4862); Phone: +86-18202988666; Email: [lyna@mail.xjtu.edu.cn](mailto:lyna@mail.xjtu.edu.cn)

### Authors

Qinlan Luo – State Key Laboratory of Multiphase Flow in Power Engineering, Xi'an Jiaotong University, Xi'an 710049, China; Joint International Center for  $\text{CO}_2$  Capture and Storage (iCCS), Hunan Provincial Key Laboratory for Cost-Effective Utilization of Fossil Fuel Aimed at Reducing  $\text{CO}_2$

Emissions, College of Chemistry and Chemical Engineering, Hunan University, Changsha 410082, China

Qulan Zhou – State Key Laboratory of Multiphase Flow in Power Engineering, Xi'an Jiaotong University, Xi'an 710049, China

Bin Feng – Xi'an Thermal Power Research Institute Co., Ltd., Xi'an 710054, China

Shicheng Liu – State Key Laboratory of Multiphase Flow in Power Engineering, Xi'an Jiaotong University, Xi'an 710049, China

Complete contact information is available at:  
<https://pubs.acs.org/10.1021/acs.iecr.1c04123>

## Notes

The authors declare no competing financial interest.

## ACKNOWLEDGMENTS

This work is supported by Science and Technology Program of Shaanxi, China (2020JM-081) and Instrumental Analysis Center of Xi'an Jiaotong University. Helpful discussions with Gyeong S. Hwang (the University of Texas, at Austin) and assistance with calculations from Bohak Yoon (the University of Texas, at Austin) are greatly acknowledged.

## REFERENCES

- (1) Zhao, B.; Liu, F.; Cui, Z.; et al. Enhancing the energetic efficiency of MDEA/PZ-based CO<sub>2</sub> capture technology for a 650 MW power plant: Process improvement. *Applied Energy*. **2017**, *185*, 362–375.
- (2) Rochelle, G. T. Amine scrubbing for CO<sub>2</sub> capture. *Science* **2009**, *325*, 1652–1654.
- (3) Schäffer, A.; Brechtel, K.; Scheffknecht, G. Comparative study on differently concentrated aqueous solutions of MEA and TETA for CO<sub>2</sub> capture from flue gases. *Fuel* **2012**, *101*, 148–153.
- (4) Zhang, R.; Zhang, X.; Yang, Q.; Yu, H.; Liang, Z.; Luo, X. Analysis of the reduction of energy cost by using MEA-MDEA-PZ solvent for post-combustion carbon dioxide capture (PCC). *Applied Energy*. **2017**, *205*, 1002–1011.
- (5) Dash, S. K.; Samanta, A.; Samanta, A. N.; Bandyopadhyay, S. S. Vapour liquid equilibria of carbon dioxide in dilute and concentrated aqueous solutions of piperazine at low to high pressure. *Fluid Phase Equilib.* **2011**, *300*, 145–154.
- (6) Derks, P. W. J.; Kleingeld, T.; van Aken, C.; Hogendoorn, J. A.; Versteeg, G. F. Kinetics of absorption of carbon dioxide in aqueous piperazine solutions. *Chem. Eng. Sci.* **2006**, *61*, 6837–6854.
- (7) Rochelle, G.; Chen, E.; Freeman, S.; Van Wagener, D.; Xu, Q.; Voice, A. Aqueous piperazine as the new standard for CO<sub>2</sub> capture technology. *Chem. Eng. J.* **2011**, *171*, 725–733.
- (8) Tong, D.; Maitland, G. C.; Trusler, M. J. P.; Fennell, P. S. Solubility of carbon dioxide in aqueous blends of 2-amino-2-methyl-1-propanol and piperazine. *Chem. Eng. Sci.* **2013**, *101*, 851–864.
- (9) Sun, W.-C.; Yong, C.-B.; Li, M.-H. Kinetics of the absorption of carbon dioxide into mixed aqueous solutions of 2-amino-2-methyl-1-propanol and piperazine. *Chem. Eng. Sci.* **2005**, *60*, 503–516.
- (10) Nwaoha, C.; Saiwan, C.; Tontiwachwuthikul, P.; et al. Carbon dioxide (CO<sub>2</sub>) capture: absorption-desorption capabilities of 2-amino-2-methyl-1-propanol (AMP), piperazine (PZ) and monoethanolamine (MEA) tri-solvent blends. *Journal of Natural Gas Science and Engineering*. **2016**, *33*, 742–750.
- (11) Nwaoha, C.; Idem, R.; Supap, T.; et al. Heat duty, heat of absorption, sensible heat and heat of vaporization of 2-Amino-2-Methyl-1-Propanol (AMP), Piperazine (PZ) and Monoethanolamine (MEA) tri-solvent blend for carbon dioxide (CO<sub>2</sub>) capture. *Chem. Eng. Sci.* **2017**, *170*, 26–35.
- (12) Du, Y.; Yuan, Y.; Rochelle, G. T. Capacity and absorption rate of tertiary and hindered amines blended with piperazine for CO<sub>2</sub> capture. *Chem. Eng. Sci.* **2016**, *155*, 397–404.
- (13) Ballard, M.; Bown, M.; James, S.; Yang, Q. NMR studies of mixed amines. *Energy Procedia*. **2011**, *4*, 291–298.
- (14) Puxty, G.; Rowland, R. Modeling CO<sub>2</sub> mass transfer in amine mixtures: PZ-AMP and PZ-MDEA. *Environ. Sci. Technol.* **2011**, *45*, 2398–2405.
- (15) Lee, B.; Stowe, H. M.; Lee, K. H.; et al. Understanding CO<sub>2</sub> capture mechanisms in aqueous hydrazine via combined NMR and first-principles studies. *Phys. Chem. Chem. Phys.* **2017**, *19*, 24067–24075.
- (16) Ciftja, A. F.; Hartono, A.; Svendsen, H. F. Experimental study on carbamate formation in the AMP–CO<sub>2</sub>–H<sub>2</sub>O system at different temperatures. *Chem. Eng. Sci.* **2014**, *107*, 317–327.
- (17) Shamair, Z.; Habib, N.; Gilani, M. A.; Khan, A. L. Theoretical and experimental investigation of CO<sub>2</sub> separation from CH<sub>4</sub> and N<sub>2</sub> through supported ionic liquid membranes. *Applied Energy* **2020**, *268*, 115016.
- (18) Jackson, P.; Beste, A.; Attalla, M. Insights into amine-based CO<sub>2</sub> capture: an ab initio self-consistent reaction field investigation. *Struct. Chem.* **2011**, *22*, 537–549.
- (19) Gangarapu, S.; Wierda, G. J.; Marcelis, A. T. M.; Zuilhof, H. Quantum chemical studies on solvents for post-combustion carbon dioxide capture: calculation of pKa and carbamate stability of disubstituted piperazines. *ChemPhysChem* **2014**, *15*, 1880–1886.
- (20) Zhang, T.; Yu, Y.; Zhang, Z. An interactive chemical enhancement of CO<sub>2</sub> capture in the MEA/PZ/AMP/DEA binary solutions. *International Journal of Greenhouse Gas Control*. **2018**, *74*, 119–129.
- (21) Leung, K.; Nielsen, I. M. B.; Kurtz, I. AbInitio Molecular Dynamics Study of Carbon Dioxide and Bicarbonate Hydration and the Nucleophilic Attack of Hydroxide on CO<sub>2</sub>. *J. Phys. Chem. B* **2007**, *111*, 4453–4459.
- (22) Kubota, Y.; Bucko, T. Carbon dioxide capture in 2,2'-iminodiethanol aqueous solution from ab initio molecular dynamics simulations. *J. Chem. Phys.* **2018**, *149*, 224103.
- (23) Hwang, G. S.; Stowe, H. M.; Paek, E.; Manogaran, D. Reaction mechanisms of aqueous monoethanolamine with carbon dioxide: a combined quantum chemical and molecular dynamics study. *Phys. Chem. Chem. Phys.* **2015**, *17*, 831–839.
- (24) Ma, C.; Pietrucci, F.; Andreoni, W. Capture and Release of CO<sub>2</sub> in Monoethanolamine Aqueous Solutions: New Insights from First-Principles Reaction Dynamics. *J. Chem. Theory Comput.* **2015**, *11*, 3189–3198.
- (25) Ma, C.; Pietrucci, F.; Andreoni, W. Reaction dynamics of CO<sub>2</sub> in aqueous amines from ab initio molecular dynamics: 2-amino-2-methyl-1,3-propanediol (AMPD) compared to monoethanolamine (MEA). *Theor. Chem. Acc.* **2016**, *135* (), DOI: 10.1007/s00214-016-1834-8.
- (26) Yoon, B.; Hwang, G. S. Anomalous Facile Carbamate Formation at High Stripping Temperatures from Carbon Dioxide Reaction with 2-Amino-2-methyl-1-propanol in Aqueous Solution. *ACS Sustainable Chem. Eng.* **2020**, *8*, 18671–18677.
- (27) Stowe, H. M.; Hwang, G. S. Molecular insights into the enhanced rate of CO<sub>2</sub> absorption to produce bicarbonate in aqueous 2-amino-2-methyl-1-propanol. *Phys. Chem. Chem. Phys.* **2017**, *19*, 32116–32124.
- (28) Luo, Q.; Cao, Y.; Liu, Z.; Feng, B.; Zhou, Q.; Li, N. A feasible process for removal and utilization of CO<sub>2</sub> in thermal power plants by MDEA + DMSO scrubbing and Cu/TiO<sub>2</sub> photocatalytic reduction. *Appl. Therm. Eng.* **2019**, *153*, 369–378.
- (29) Luo, Q.; Feng, B.; Liu, Z.; Zhou, Q.; Zhang, Y.; Li, N. Experimental study on simultaneous absorption and desorption of CO<sub>2</sub>, SO<sub>2</sub>, and NO<sub>x</sub> using aqueous n-methyldiethanolamine and dimethyl sulfoxide solutions. *Energy Fuels* **2018**, *32*, 3647–3659.
- (30) Holmes, P. E.; Naaz, M.; Poling, B. E. Ion Concentrations in the CO<sub>2</sub>–NH<sub>3</sub>–H<sub>2</sub>O System from 13C NMR Spectroscopy. *Ind. Eng. Chem. Res.* **1998**, *37*, 3281–3287.



- (31) Jakobsen, J. P.; Krane, J.; Svendsen, H. F. Liquid-Phase Composition Determination in CO<sub>2</sub>–H<sub>2</sub>O–Alkanolamine Systems: An NMR Study. *Ind. Eng. Chem. Res.* **2005**, *44*, 9894–9903.
- (32) *Gaussian 09*; [computer program]. Version Revision A.02. Gaussian, Inc.: Wallingford CT, 2016.
- (33) Marenich, A. V.; Cramer, C. J.; Truhlar, D. G. Universal solvation model based on solute electron density and on a continuum model of the solvent defined by the bulk dielectric constant and atomic surface tensions. *J. Phys. Chem. B* **2009**, *113*, 6378–6396.
- (34) Yoon, B.; Stowe, H. M.; Hwang, G. S. Molecular mechanisms for thermal degradation of CO<sub>2</sub>-loaded aqueous monoethanolamine solution: a first-principles study. *Phys. Chem. Chem. Phys.* **2019**, *21*, 22132–22139.
- (35) Laasonen, K.; Pasquarello, A.; Car, R.; Lee, C.; Vanderbilt, D. Car-Parrinello molecular dynamics with Vanderbilt ultrasoft pseudopotentials. *Phys. Rev. B: Condens. Matter* **1993**, *47*, 10142–10153.
- (36) Car, R.; Parrinello, M. Unified approach for molecular dynamics and density-functional theory. *Phys. Rev. Lett.* **1985**, *55*, 2471–2474.
- (37) Valsson, O.; Parrinello, M. Variational approach to enhanced sampling and free energy calculations. *Phys. Rev. Lett.* **2014**, *113*, 090601.
- (38) Zhang, Y.; Yang, W. Comment on Generalized Gradient Approximation Made Simple. *Phys. Rev. Lett.* **1998**, *80*, 890–890.
- (39) Wai, S. K.; Nwaoha, C.; Saiwan, C.; Idem, R.; Supap, T. Absorption heat, solubility, absorption and desorption rates, cyclic capacity, heat duty, and absorption kinetic modeling of AMP–DETA blend for post-combustion CO<sub>2</sub> capture. *Sep. Purif. Technol.* **2018**, *194*, 89–95.
- (40) Guo, C.; Chen, S.; Zhang, Y. A <sup>13</sup>C NMR study of carbon dioxide absorption and desorption in pure and blended 2-(2-aminoethylamine)ethanol (AEEA) and 2-amino-2-methyl-1-propanol (AMP) solutions. *Int. J. Greenhouse Gas Control* **2014**, *28*, 88–95.
- (41) Ciftja, A. F.; Hartono, A.; Svendsen, H. F. Carbamate Stability Measurements in Amine/CO<sub>2</sub>/Water Systems with Nuclear Magnetic Resonance (NMR) Spectroscopy. *Energy Procedia.* **2014**, *63*, 633–639.
- (42) Liu, H.; Li, M.; Luo, X.; Liang, Z.; Idem, R.; Tontiwachwuthikul, P. Investigation mechanism of DEA as an activator on aqueous MEA solution for postcombustion CO<sub>2</sub> capture. *AIChE J.* **2018**, *64*, 2515–2525.
- (43) Perinu, C.; Arstad, B.; Jens, K.-J. NMR spectroscopy applied to amine–CO<sub>2</sub>–H<sub>2</sub>O systems relevant for post-combustion CO<sub>2</sub> capture: A review. *International Journal of Greenhouse Gas Control* **2014**, *20*, 230–243.
- (44) Ciftja, A. F.; Hartono, A.; Svendsen, H. F. <sup>13</sup>C NMR as a method species determination in CO<sub>2</sub> absorbent systems. *International Journal of Greenhouse Gas Control* **2013**, *16*, 224–232.
- (45) Stowe, H. M.; Paek, E.; Hwang, G. S. First-principles assessment of CO<sub>2</sub> capture mechanisms in aqueous piperazine solution. *Phys. Chem. Chem. Phys.* **2016**, *18*, 25296–25307.
- (46) Astarita, G.; Savage, D. W.; Longo, J. M. Promotion of CO<sub>2</sub> mass transfer in carbonate solutions. *Chem. Eng. Sci.* **1981**, *36*, 581–588.
- (47) Böttinger, W.; Maiwald, M.; Hasse, H. Online NMR spectroscopic study of species distribution in MEA–H<sub>2</sub>O–CO<sub>2</sub> and DEA–H<sub>2</sub>O–CO<sub>2</sub>. *Fluid Phase Equilib.* **2008**, *263*, 131–143.
- (48) Fan, G.-j.; Wee, A. G. H.; Idem, R.; Tontiwachwuthikul, P. NMR Studies of Amine Species in MEA–CO<sub>2</sub>–H<sub>2</sub>O System: Modification of the Model of Vapor–Liquid Equilibrium (VLE). *Ind. Eng. Chem. Res.* **2009**, *48*, 2717–2720.
- (49) Shi, H.; Naami, A.; Idem, R.; Tontiwachwuthikul, P. 1D NMR Analysis of a Quaternary MEA–DEAB–CO<sub>2</sub>–H<sub>2</sub>O Amine System: Liquid Phase Speciation and Vapor–Liquid Equilibria at CO<sub>2</sub> Absorption and Solvent Regeneration Conditions. *Ind. Eng. Chem. Res.* **2014**, *53*, 8577–8591.
- (50) Shi, H.; Zheng, L.; Huang, M.; et al. CO<sub>2</sub> desorption tests of blended monoethanolamine-diethanolamine solutions to discover novel energy efficient solvents. *Asia-Pac. J. Chem. Eng.* **2018**, *13*, No. e2186.
- (51) Said, R. B.; Kolle, J. M.; Essalah, K.; Tangour, B.; Sayari, A. A Unified Approach to CO<sub>2</sub>-Amine Reaction Mechanisms. *ACS Omega* **2020**, *5*, 26125–26133.
- (52) Davran-Candan, T. DFT modeling of CO<sub>2</sub> interaction with various aqueous amine structures. *J. Phys. Chem. A* **2014**, *118*, 4582–4590.
- (53) Stowe, H. M.; Hwang, G. S. Fundamental understanding of CO<sub>2</sub> capture and regeneration in aqueous amines from first-principles studies: recent progress and remaining challenges. *Ind. Eng. Chem. Res.* **2017**, *56*, 6887–6899.
- (54) Hamborg, E. S.; Versteeg, G. F. Dissociation constants and thermodynamic properties of amines and alkanolamines from 293 to 353 K. *J. Chem. Eng. Data* **2009**, *54*, 1318–1328.
- (55) Littel, R.; Bos, M.; Knoop, G. J. Dissociation constants of some alkanolamines at 293, 303, 318, and 333 K. *J. Chem. Eng. Data* **1990**, *35*, 276–277.
- (56) Shi, H.; Naami, A.; Idem, R.; Tontiwachwuthikul, P. Catalytic and non catalytic solvent regeneration during absorption-based CO<sub>2</sub> capture with single and blended reactive amine solvents. *International Journal of Greenhouse Gas Control* **2014**, *26*, 39–50.
- (57) Xie, H.-B.; Zhou, Y.; Zhang, Y.; Johnson, J. K. Reaction Mechanism of Monoethanolamine with CO<sub>2</sub> in Aqueous Solution from Molecular Modeling. *J. Phys. Chem. A* **2010**, *114*, 11844–11852.

## Recommended by ACS

### Impact of Hydrogen Bonds on CO<sub>2</sub> Binding in Eutectic Solvents: An Experimental and Computational Study toward Sorbent Design for CO<sub>2</sub> Capture

Aidan Klemm, Burcu Gurkan, *et al.*

FEBRUARY 17, 2023

ACS SUSTAINABLE CHEMISTRY & ENGINEERING

READ 

### Porous Polymer Supported Amino Functionalized Ionic Liquid for Effective CO<sub>2</sub> Capture

Jianmeng Wu, Hui Yang, *et al.*

FEBRUARY 07, 2023

LANGMUIR

READ 

### Theoretical Analysis of Physical and Chemical CO<sub>2</sub> Absorption by Tri- and Tetraepoxidized Imidazolium Ionic Liquids

Luke Wylie, Agilio Padua, *et al.*

NOVEMBER 16, 2022

THE JOURNAL OF PHYSICAL CHEMISTRY B

READ 

### High-Loading Poly(ethylene glycol)-Blended Poly(acrylic acid) Membranes for CO<sub>2</sub> Separation

Somi Yu, Won Seok Chi, *et al.*

JANUARY 06, 2023

ACS OMEGA

READ 

Get More Suggestions >